BIOPHYSICS

# Topology-dependent anomalous dynamics of ring and linear DNA are sensitive to cytoskeleton crosslinking

**Devynn M. Wulstein*, Kathryn E. Regan*, Jonathan Garamella, Ryan J. McGorty†, Rae M. Robertson-Anderson†‡**



**Cytoskeletal crowding plays a key role in the diffusion of DNA molecules through the cell, acting as a barrier to effective intracellular transport and conformational stability required for processes such as transfection, viral infection, and gene therapy. Here, we elucidate the transport properties and conformational dynamics of linear and ring DNA molecules diffusing through entangled and crosslinked composite networks of actin and microtubules. We couple single-molecule conformational tracking with differential dynamic microscopy to reveal that ring and linear DNA exhibit unexpectedly distinct transport properties that are influenced differently by cytoskeleton crosslinking. Ring DNA coils are swollen and undergo heterogeneous and biphasic subdiffusion that is hindered by crosslinking. Conversely, crosslinking actually facilitates the single-mode subdiffusion that compacted linear chains exhibit. Our collective results demonstrate that transient threading by cytoskeleton filaments plays a key role in the dynamics of ring DNA, whereas the mobility of the cytoskeleton dictates transport of linear DNA.**

## INTRODUCTION

DNA, a ubiquitous biopolymer in eukaryotic and prokaryotic cells, occurs naturally in linear and relaxed circular (ring) topologies. Transport of these topologically distinct biopolymers through the cytoskeleton is crucial for a wide range of processes and functions such as transcription, transformation, looping, gene expression, and gene therapy (*1*–*5*). However, the cytoskeleton is a crowded composite network of filamentous proteins that can restrict transport and affect the conformational stability of DNA required for these diverse processes (*6*–*8*). Two primary cytoskeletal proteins are semiflexible actin filaments with a persistence length $l_p \approx 10$ μm and rigid microtubules with $l_p \approx 1$ mm (*6*, *8*–*10*). These biopolymers form steric entanglements with one another and are also often chemically crosslinked via accessory proteins to enable proliferation, differentiation, and cell migration (*8*, *10*–*13*). The role that crosslinking plays in the viscoelastic properties of in vitro actin and microtubule networks has been widely studied (*10*, *11*, *14*). More recently, the interactions between actin and microtubules and their role in cell mechanics have begun to be explored (*15*–*19*). However, far less understood is the dynamics, both center-of-mass and conformational, of biopolymers such as DNA existing within these composite cytoskeletal networks (*19*).

Cellular crowding has long been recognized as playing a key role in intracellular transport and conformational dynamics, and numerous studies have been devoted to understanding the complex and often anomalous diffusive properties that arise in these environments (*20*–*27*). However, the vast parameter space of crowding conditions and diffusing biopolymers and particles of interest has led to wide-ranging experimental results and theoretical predictions (*24*, *28*). Several of these studies have reported normal Brownian motion in which the mean squared displacement (MSD) scales linearly with time as MSD ~ $2Dt$, where $D$ is the diffusion coefficient (*22*, *27*, *29*, *30*). Others have reported anomalous subdiffusion, in which the MSD scales as a power law with time, MSD ~ $Kt^{\alpha}$, where $K$ is the transport coefficient and the scaling exponent $\alpha < 1$ (*19*–*21*, *24*, *25*, *31*–*34*). Crowded DNA and other polymers have also been reported to undergo compaction, swelling, or elongation depending on the topology and size of the DNA and crowders (*20*, *21*, *35*, *36*). However, in most of these studies, the crowders have been small globular proteins or synthetic polymers that cannot accurately mimic the constraints the cytoskeleton imposes.

When the crowders are sufficiently long and concentrated, as is the case for the cytoskeleton, they become entangled, and their mobility is restricted. These entangled networks affect the diffusion and conformation of tracers differently from systems of small mobile crowders. Likewise, distinct from the dynamics of spherical tracer particles, long tracer polymers such as DNA embedded in an entangled network are restricted to move via curvilinear diffusion along their backbones—a process termed reptation (*37*, *38*). However, ring polymers lack free ends required for this "head-first" diffusive mechanism. Hence, transport of rings through entangled and crowded networks is fundamentally different than linear chain transport and is thus a topic of great current interest and debate (*39*–*46*).

Ring polymers entangled by linear chains have been predicted to assume diverse conformations that lead to multiple transport mechanisms (*34*, *46*–*53*). They can be folded in half and undergo reptation-like diffusion similar to a linear chain of half the length, or adopt amoeba-like conformations that diffuse similar to branched polymers. Rings can also become threaded by surrounding linear chains such that they can only diffuse by the threading chains unthreading via reptation, a process termed constraint release. This extremely slow process is essentially halted if the threading chains are crosslinked and thus cannot reptate to unthread the ring and release the constraint they impose. Simulations have shown that these multiple

Department of Physics and Biophysics, University of San Diego, San Diego, CA 92110, USA.
*These authors contributed equally to this work.
†These authors contributed equally to this work.
‡Corresponding author. Email: randerson@sandiego.edu

diffusive modes, and the interconversion between them, lead to heterogeneous transport and conformations of rings (*54*–*56*). However, experimental evidence for these varied transport modes and conformations is sparse (*49*, *50*, *57*). Further, how these idealized models translate to complex biological systems, such as DNA diffusion through the cytoskeleton, remains unknown.

Here, we couple single-molecule conformational tracking (SMCT) with differential dynamic microscopy (DDM) to characterize the dynamics of linear and ring DNA molecules crowded by entangled and crosslinked cytoskeletal networks. We find intriguing dependences of both DNA topology and cytoskeleton crosslinking on the transport and conformational dynamics of DNA over a range of spatiotemporal scales. Ring DNA exhibits biphasic subdiffusion and slow fluctuations between a broad range of swollen conformational states and corresponding transport modes. Linear DNA undergoes faster single-mode diffusion and more compact conformations with a narrow distribution of dynamical modes. Further, while crosslinking suppresses ring DNA diffusion, it enhances the diffusion of linear DNA. Lastly, ensemble analysis reveals that, unlike linear DNA, rings undergo highly heterogeneous transport that cannot be fit to standard models of diffusion. These collective results suggest that threading—inaccessible to linear chains—plays a key role in the transport of ring DNA within cytoskeleton networks. Beyond the importance of our results to biological processes such as transfection, infection, and gene therapy, our work also provides key insights into the dynamics of entangled ring polymers—a topic of broad current interest (*49*, *54*, *58*–*60*).

## RESULTS

As detailed in Fig. 1 and Materials and Methods, the ring and linear DNA used in our experiments have identical contour lengths of $L \cong$ 38 μm [115 kilobase pairs (kbp)] and topology-dependent mean end-to-end coil lengths of $R_{0,R} \cong 1.6$ μm and $R_{0,L} \cong 2.6$ μm. The cytoskeleton networks both have a mesh size of $\xi \cong 0.81$ μm, and in the crosslinked network, every filament crossing or entanglement can be assumed to be crosslinked. The longest relaxation times for entangled and crosslinked networks have been reported to be ~3.3 and ~4.1 s (*16*), similar to our measurement time scale for single-molecule tracking.

We use SMCT to examine the effect of crosslinking on the dynamics of ring and linear DNA molecules diffusing within the described cytoskeleton networks (Fig. 1). We track the center-of-mass (COM) trajectories of an ensemble of individual molecules from which we evaluate MSDs (see Materials and Methods, Fig. 2A, and fig. S1). As shown in Fig. 2A, the MSDs are sublinear (i.e., subdiffusive), so we fit MSDs to the power-law function MSD = $Kt^{\alpha}$, where $K$ is the transport coefficient and α is the anomalous scaling exponent (Fig. 2, B and C). As described in Introduction, for normal Brownian motion, α = 1 and $K = 2D$, where $D$ is the diffusion coefficient.

As shown in Fig. 2, we observe a clear difference in the MSDs for ring and linear DNA in both entangled (E) and crosslinked (XL) networks. For both network architectures, ring DNA exhibits lower transport coefficients and a higher degree of subdiffusion. This behavior is in contrast to dilute conditions in which ring DNA diffuses ~1.4× faster than its linear counterpart due to its smaller conformational size (i.e., radius of gyration $R_G$) and reduced degrees of freedom (*46*). Further, while MSDs for linear DNA obey a single subdiffusive power law (α ≈ 0.73), ring DNA MSDs display an intriguing shift from α ≈ 0.65 scaling to a more subdiffusive regime (α ≈ 0.48) at ~0.4 μm$^2$ (Fig. 2A). These topology-dependent differences are amplified when crosslinkers are added to the networks. As shown in Fig. 2 (B and C), rings and linear chains exhibit opposite responses to crosslinking. Namely, ring DNA transport becomes slower (decrease in $K$) and more anomalous (decrease in α), while linear DNA undergoes faster, less anomalous motion (increase in $K$ and α). We also evaluate the distribution of time-averaged MSDs of individual molecules (fig. S1). We find that these distributions are wider for ring DNA compared to linear DNA in both network types. Further, the distribution for rings includes a fraction of nearly zero MSDs, particularly in the crosslinked network. This effect is absent in the linear DNA distributions.

To shed further light on the topology-specific differences in transport, we quantify the distributions of conformational states accessed by ring and linear DNA molecules in both network types. Specifically, as described in Materials and Methods and Fig. 1B, we calculate an effective DNA coil size, $R_{coil} = [1/2(R_{max}^2 + R_{min}^2)]^{1/2}$, and normalize by the dilute limit mean end-to-end length, $R_0 = \sqrt{6}\,R_G$ (*61*). Probability distributions of this reduced coil size $r_{coil}$ (Fig. 3A), as well as the mean value $\langle r_{coil} \rangle$ (Fig. 3B and table S1) and full width at half maximum (FWHM; Fig. 3C and table S1), show distinct differences between the two topologies. Specifically, linear DNA conformations are more compact than their dilute limit size (i.e., $r_{coil} < 1$), while ring DNA is swollen ($r_{coil} > 1$). The width of ring DNA distributions, quantified by the FWHM, is also markedly larger than for linear DNA, signifying a greater range of conformational states assumed by rings compared to linear DNA. This effect mirrors that of the transport distributions shown in fig. S1. Crosslinking the composite networks increases $\langle r_{coil} \rangle$ for both topologies, yet its impact on the range of conformations accessed (i.e., FWHM) is topology dependent. Namely, for linear DNA, there is little change in the FWHM upon crosslinking, whereas crosslinking reduces the FWHM for ring DNA.

The topology-dependent breadth in conformations, quantified by the FWHM, can arise from a heterogeneous ensemble of molecules that have different conformational states, from a homogenous ensemble in which all molecules undergo large conformational fluctuations in time, or from a combination of both. To determine which, if any, of these possibilities is dominant, we determine the extent to which molecules conformationally fluctuate or "breathe" between different conformational states. Specifically, for each tracked molecule, we measure the fractional change in $R_{max}$ between varying lag times $t$, which we term the fractional fluctuation length, $L_f(t) = \langle |R_{max}(0) - R_{max}(t)| \rangle / \langle R_{max} \rangle$ (Fig. 3D). For the case of a heterogeneous ensemble of largely static conformations, the asymptotic value of $L_f(t)$ should be small and not correlate with the FWHM of the DNA coil size distribution, whereas for a temporally fluctuating homogenous sample, the FWHM should be proportional to the asymptotic $L_f(t)$ value. For linear DNA, $L_f(t)$ approaches a steady-state plateau value over the measurement time scale, whereas ring DNA fluctuations are much slower, with $L_f(t)$ following power-law scaling over the entire measurement time. To better quantify the characteristic time and scale of conformational fluctuations, we calculate the final fractional fluctuation length $L_{f,f}$ and the time τ needed to reach 90% of $L_{f,f}$ (Fig. 3E and table S1). Not only do rings fluctuate more slowly (i.e., larger τ) but also the scale of fluctuations $L_{f,f}$ is smaller than for linear DNA. Thus, the effective fluctuation speed $L_{f,f}\,\tau^{-1}$ for rings is 62 and 35% slower than for linear DNA in entangled and crosslinked networks, respectively. Given the ~2-fold

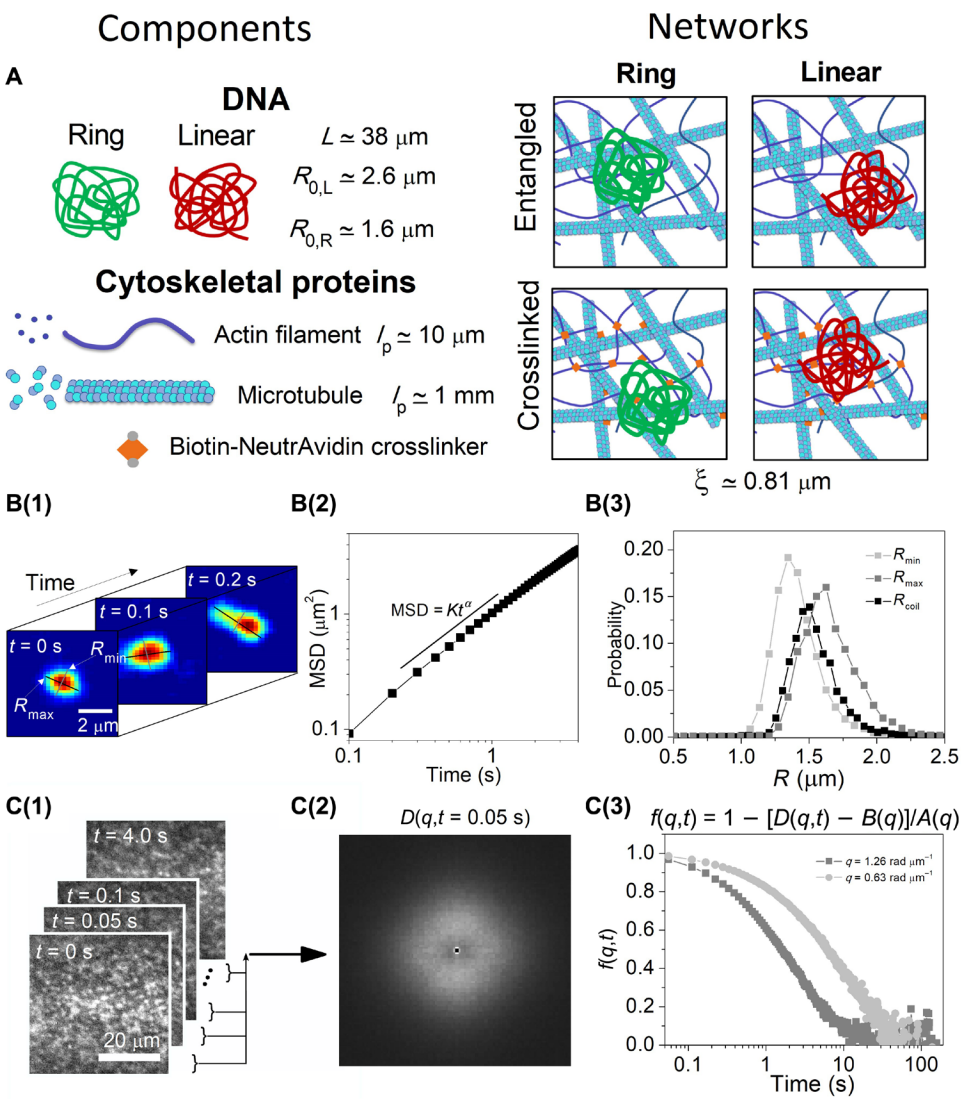


**Fig. 1. Experimental approach to elucidating the effect of DNA topology on the transport and conformational properties of DNA diffusing through model cytoskeleton composites.** (**A**) Cartoon of fluorescent-labeled 115-kbp ring and linear DNA molecules embedded in composite networks of actin and microtubules that are either entangled or crosslinked by biotin-NeutrAvidin crosslinkers. $L$ is the DNA contour length, $R_0$ is the topology-dependent mean end-to-end length of the DNA coils, $l_p$ is persistence length, and ξ is the composite mesh size. Not drawn to scale. (**B**) Single-molecule analysis (1) tracks the center-of-mass (COM) position and the lengths of the major and minor axes ($R_{max}$ and $R_{min}$) of each DNA molecule for every frame of the time series to quantify the transport and conformational dynamics of individual DNA molecules. From (1), the COM MSD (2) and probability distributions of $R_{max}$, $R_{min}$, and $R_{coil} = [½(R_{max}^2 + R_{min}^2)]^{1/2}$ (3) are computed. (**C**) From the differences in images separated by a given lag time (1), DDM analysis computes the matrix $D(q,t)$, where $q$ is the magnitude of the wave vector (2). The intermediate scattering functions (ISFs) $f(q,t)$ versus lag time for each spatial frequency $q$ describes the ensemble dynamics (3).

larger FWHM of coil size distributions for rings compared to linear DNA (Fig. 3C), this result suggests that the distribution of conformational states for rings arises from a heterogenous ensemble of ring molecules, assuming different conformational states rather than rings undergoing enhanced conformational fluctuations in time compared to linear DNA. Further, crosslinking decreases $L_{f,f}$ and increases τ for both DNA topologies, indicating that the corresponding reduction in FWHM of rings upon crosslinking arises from suppressed fluctuations or interconversion between states rather than a reduction in the number of states the molecules access. Lastly, while crosslinking amplifies the differences in COM transport dynamics between ring and linear DNA, it unexpectedly gives rise to more similar conformational dynamics between topologies. Specifically, as shown in Fig. 3 (B to E), the topology-dependent differences between the derived quantities $<r_{coil}>$, FWHM, $L_{f,f}$, and τ are all less in crosslinked compared to entangled networks.

We show above that the larger breadth in $r_{coil}$ distributions for rings versus linear chains comes from a more heterogeneous ensemble of conformational states rather than larger conformational fluctuations in time. We argue that these conformational states, which could, for example, be predicted threaded, folded, and amoeba-like states for rings, are linked to different transport modes such as reptation, restricted reptation, constraint release, caged diffusion, etc. (*49*, *54*). To verify this interpretation, we turn to our DDM analysis (Fig. 1C and Materials and Methods), which measures the decay of density fluctuations of labeled DNA within the sample to

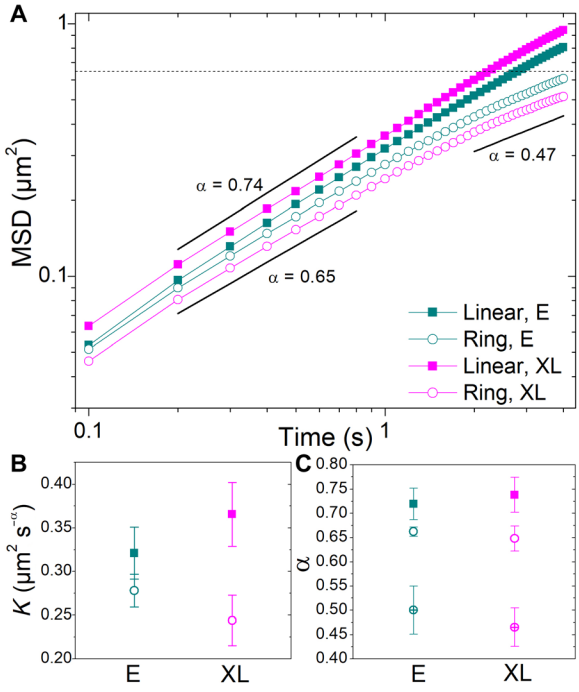


**Fig. 2. Ring DNA in cytoskeleton composites exhibits unique two-phase subdiffusion distinct from linear DNA and amplified by cytoskeleton crosslinking.** (**A**) MSDs versus time for ring (open circles) and linear (closed squares) DNA in entangled (cyan; E) and crosslinked (magenta; XL) actin-microtubule networks. Horizontal dashed line denotes where MSD = $\xi^2$. Black lines represent power-law scaling with exponents listed. Fits of the MSDs to the power-law relation MSD = $Kt^{\alpha}$ yield transport coefficients $K$ (**B**) and scaling exponents $\alpha$ (**C**) for linear (closed squares) and ring (open and crossed circles) DNA. MSDs for linear DNA obey a single power law over the entire measurement time [squares in (C)], while rings exhibit a second slower phase with lower $\alpha$ values [crossed circles in (C)] starting at ~0.4 μm$^2$. (C) Linear DNA exponents are determined from fits over $t$ = 0.1 to 4 s (closed squares), while ring DNA exhibits two different exponents with values determined from fits over $t$ = 0.1 to 2 s (open circles) and $t$ = 2 to 4 s (crossed circles). As shown, linear DNA exhibits faster transport and less subdiffusion in crosslinked compared to entangled networks, while crosslinking has the opposite effect on ring DNA.

probe the transport of large subensembles of molecules over ~5× longer times than with SMCT (*62*).

By evaluating the intermediate scattering functions (ISFs) for all conditions, we determine the extent to which transport is heterogeneous and how long anomalous dynamics persist. As shown in Fig. 4A, ring transport is significantly slower than that for linear DNA, displayed as a much slower decay of the ISF and larger ISF values for all times. In addition, while the ISF for linear DNA follows a nearly exponential decay, expected for diffusive dynamics (*19*, *63*) and well fit to standard models for subdiffusion, the ISF for ring DNA is far from a simple exponential and cannot be fit to any existing models used to analyze DDM ISFs (*62*–*66*). These data corroborate our SMCT results, which show that rings exhibit much slower and more anomalous transport than linear DNA, and further suggest the existence of multiple modes of transport. Further, the response of the DNA to network crosslinking is topology dependent. Ring DNA ISFs decay more slowly in crosslinked versus entangled networks, similar to our SMCT results that show a decrease in $K$ and $\alpha$ values upon crosslinking. On the other hand, linear DNA exhibits nearly identical ISFs in the two network architectures, compared to the corresponding SMCT results that show the measured MSD and corresponding $K$ and $\alpha$ values increase upon crosslinking. Because DDM measures density fluctuations that can arise from both conformational fluctuations and COM transport, the increase in COM transport of linear DNA with crosslinking coupled with the corresponding decrease in conformational fluctuations may explain the similarity between the linear DNA ISFs for both network architectures. Conversely, for rings, we see a decrease in both COM transport and conformational dynamics with crosslinking, which accounts for the different ISFs.

To evaluate the heterogeneity in transport modes, we consider the spread in ISFs over different spatial regions of interest (ROIs) of the network (Fig. 4, B and C). Specifically, a wider spread in the distribution of individual ISFs (gray lines) indicates more heterogeneity in transport modes. To quantify this heterogeneity, we compute the difference between the maximum and minimum ISF values for each lag time, $\Delta f(t) = f_{max}(t) - f_{min}(t)$ (Fig. 4, D and E). As shown, $\Delta f(t)$ for ring DNA in both network types is significantly larger than that for linear DNA. This topology-dependent difference in ISF heterogeneity is evidence that the spread measured in the conformational analysis (Fig. 3) is linked to varying transport modes and that rings access a wider range of transport modes that are inaccessible to linear DNA. Further, we also once again see an opposite effect of crosslinking for the different topologies. Crosslinking slightly increases $\Delta f(t)$ for linear DNA while it slightly reduces $\Delta f(t)$ for rings. The reduction for rings corroborates the reduction in the FWHM of $r_{coil}$—coupling the suppression of conformational states with that of transport modes. For linear DNA, our SMCT analysis shows a ~8% reduction in $L_f(t)$ upon crosslinking but no change in the FWHM of the $r_{coil}$ distribution, which includes both temporal fluctuations and heterogeneities. To maintain the same FWHM, there must be an increase in the heterogeneity of transport modes for linear DNA to compensate for the reduced temporal fluctuations. This effect is what is demonstrated by the increase in $\Delta f(t)$ for linear DNA upon crosslinking (Fig. 4, D and E).

## DISCUSSION

Our collective results indicate that ring DNA adopts a wide range of transport modes, each with corresponding distinct conformations, that are not accessible to linear DNA (Fig. 5). These modes are accompanied by chain swelling and suppressed conformational fluctuations that are exacerbated by cytoskeleton crosslinking. As described in Introduction, ring polymers entangled by linear chains have been predicted to assume folded, amoeba-like, and threaded conformations that lead to slower diffusion of rings compared to their linear counterparts. Ring DNA tracers embedded in solutions of entangled linear DNA have been reported to have diffusion coefficients up to an order of magnitude lower than their linear DNA equivalents (*34*, *46*, *50*), a phenomenon that has been attributed to threading events. Simulations have also shown that threading leads to anomalous diffusion and swelling of DNA coils (*47*–*49*, *54*) similar to our results. Lastly, large fluctuations in the relaxation dynamics of ring DNA embedded in semidilute linear DNA solutions have recently been observed and attributed to threading events (*49*).

Further evidence of threading lies in the biphasic MSDs for rings (Fig. 2A). The length scale at which ring DNA MSDs exhibit a shift to more subdiffusive transport (~0.4 μm$^2$) is remarkably close to the

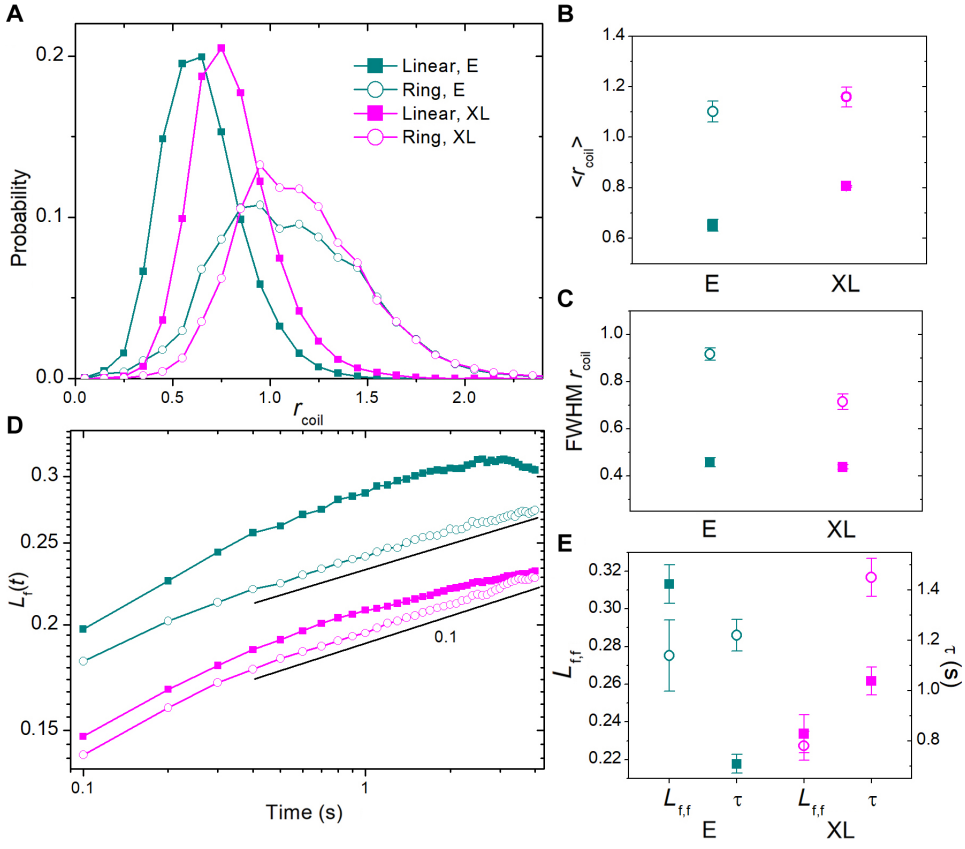


**Fig. 3. Both DNA topology and cytoskeleton crosslinking affect the conformational dynamics of ring and linear DNA in cytoskeleton composites.** (**A**) Probability distributions of the coil sizes $R_{coil}$ for every frame of every molecule. $R_{coil}$ is rescaled by the expected dilute-limit end-to-end distance $R_0$, which we denote as $r_{coil}$. Distributions show compaction of linear DNA (squares; distribution centered at <1) from normal $R_0$ values, while ring DNA (open circles) swells and accesses a broader range of coil sizes (distribution centered at >1, broader than linear DNA distributions). (**B**) Mean rescaled coil sizes $<r_{coil}>$ quantify the swelling of rings (circles) and compaction of linear DNA (squares) in entangled (E; cyan) and crosslinked (XL; magenta) networks. (**C**) FWHM of $r_{coil}$ distributions shown in (A), displaying the topology-dependent range of conformational states accessed by DNA. (**D**) Fractional fluctuation length $L_f(t) = <|R_{max}(0) - R_{max}(t)|>/<R_{max}>$ for linear and ring DNA with black lines denoting power-law scaling with exponent listed. Linear DNA fluctuates more quickly and over a larger range than ring DNA, approaching steady-state values in contrast to the slow power-law rise of ring DNA. (**E**) The final fractional fluctuation length $L_{f,f}$ plotted alongside the time τ at which molecules reach 90% of $L_{f,f}$. As shown, ring DNA fluctuates more slowly and over a smaller range than linear DNA in both entangled and crosslinked networks.

squared radius of gyration of rings $R_G^2$ = 0.42 μm (*46*). Threaded or pinned rings are restricted to move largely perpendicular to the threading filaments and thus can only readily move within a distance ~$R_G$. COM motion of threaded rings over distances larger than $R_G$ can only arise via the slow mechanism of constraint release, which presumably occurs on a time scale comparable to the longest relaxation time of the network (~3 s). Hence, this secondary slower phase in COM transport likely arises from the transport mode associated with threaded DNA being partially frozen out at distances >$R_G$. The reduction in ring transport upon crosslinking corroborates this result. Crosslinking of entangled cytoskeleton filaments limits filament diffusion and thus hinders their ability to release their constraints to allow threaded rings to diffuse. Hence, ring DNA in crosslinked networks can remain threaded for much longer periods of time—even indefinitely—leading to a higher degree of subdiffusion and decreased transport coefficients. This effect is also manifested in the MSD distribution (fig. S1) that shows a fraction of rings exhibiting nearly zero MSDs. One may have expected an even larger difference in *K* and α values upon crosslinking if, in entangled networks, rings can be released via reptation of filaments, whereas in crosslinked networks, they are confined to move <$R_G$ indefinitely. However, because the mesh size of the networks ξ is ~2 to 3× smaller than the DNA coil size (Fig. 1A), it is quite likely that many of the rings are threaded by multiple filaments or become threaded by a new filament before the original threading filament releases its constraint. This phenomenon would prolong the time over which rings remain constrained well beyond the longest relaxation time of the network. This effect also likely contributes to the lack of a long-time plateau in $L_f(t)$ for rings.

The simplified model described above ignores the fact that threaded rings could also move along the backbones of the threading filaments rather than simply perpendicular to them. However, this motion would be confined to the mesh size of the network. If a large fraction of the rings is threaded, then we would expect the MSDs to be restricted to <$\xi^2$, particularly for times less than the network relaxation time. This effect is indeed manifested in Fig. 2A in which the MSDs for rings remain <$\xi^2$ over the entire measurement, and one may argue that the curves appear to be asymptoting to $\xi^2$. Conversely, the MSDs for linear DNA surpass $\xi^2$ and display no asymptotic behavior.

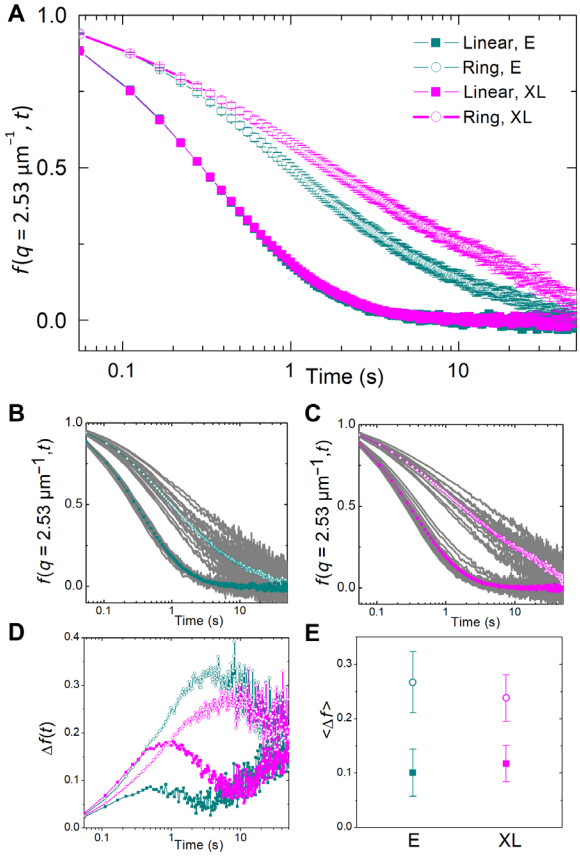


**Fig. 4. DDM reveals heterogeneous slow transport of ring DNA with unique sensitivity to crosslinking.** (**A**) Average ISF $f(q,t)$ with $q$ = 2.53 rad μm$^{-1}$ for ring (circles) and linear (squares) DNA in entangled (cyan) and crosslinked (magenta) cytoskeleton composites. Displayed curves are averages over 20 regions of interest (ROIs). ISFs for linear DNA decay much faster than for ring DNA and exhibit expected exponential decay not seen for rings. While crosslinking slows the decay for rings, it has a negligible effect on the linear DNA ISF. (**B** and **C**) All individual ISFs (gray) comprising the average ISF (color coded) for linear and ring DNA in entangled (B) and crosslinked (C) composites. The substantial spread in ISF curves for ring DNA and the slow decay to zero—both features absent for linear DNA—indicate heterogeneous or multimode transport and anomalous slow diffusion, respectively. ISFs for crosslinked networks show a slightly smaller spread for ring topologies, while the spread for linear topologies is slightly larger. (**D**) That spread in ISFs is quantified by taking the difference between the maximum and minimum values of $f(q,t)$, $\Delta f(q,t)$, among the multiple ROIs at $q$ = 2.53 rad μm$^{-1}$. (**E**) The average $\Delta f(q,t)$ over the range of time lags is greater with ring than with linear DNA for both networks. For rings, moving from an entangled to a crosslinked network decreases the spread. Conversely, for linear DNA, the spread increases slightly upon crosslinking.

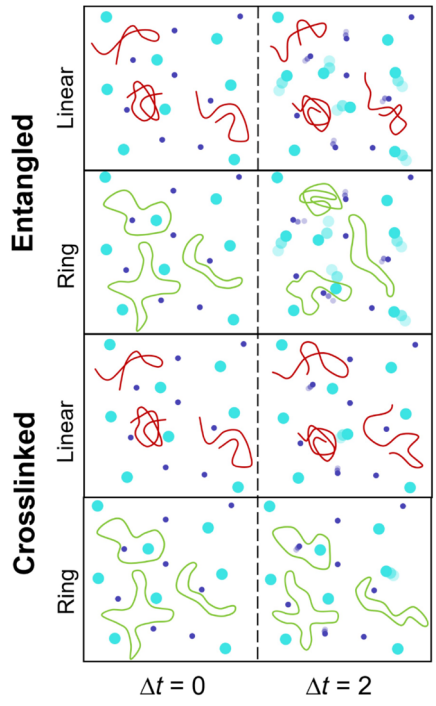


**Fig. 5. Ring DNA molecules in cytoskeleton networks adopt multiple modes of transport that are not accessible to linear DNA and are affected by cytoskeleton crosslinking.** Cartoon of ring (green) and linear (red) DNA diffusing through entangled and crosslinked networks of actin (purple) and microtubules (blue). Time scale is arbitrary, and cartoons are not drawn to scale. Each panel is a depiction of a slice in the *xy* plane with DNA aligned in the plane and actin and microtubule constraints oriented along *z*. In right-hand panels ($\Delta t$ = 2), lighter shaded circles denote the two previous positions ($\Delta t$ = 0, 1) of the corresponding constraints. Within entangled networks, linear DNA can reptate through the network, while ring DNA adopts branched, folded, or threaded conformations. Reptation of the entangled cytoskeleton filaments allows threaded rings to become unthreaded via constraint release of the threading filaments. Crosslinking suppresses the mobility of cytoskeleton filaments that can cause rings to become permanently threaded, slowing their transport, while, at the same time, increasing the mobility of linear DNA as described in text (Fig. 2).

The question remains as to why crosslinking facilitates the transport of linear DNA, given that it serves to restrict the reptation of the entangling linear cytoskeleton filaments. Further, this increased transport is coupled with larger conformations, at odds with the Newtonian Stokes relationship ($D \sim R_{coil}^{-1}$). We previously showed that linear DNA diffusing in a network of semiflexible actin filaments was more compact and displayed more extreme subdiffusion and lower transport coefficients than when diffusing in a network of more rigid microtubules (*19*). Further, recent simulations have shown that the slow mobility of large crowders, which results in continuous temporal evolution of the crowding mesh, was required for true anomalous subdiffusion (*67*). In contrast, rigid constraints (such as crosslinked filaments) resulted in less extreme transient subdiffusion arising from temporary caging of particles in the rigid mesh coupled with hopping to new pockets in the mesh. In a more mobile network, hopping is avoided because the particle motion is coupled to the crowding network motion such that it traverses voids in the mesh by the slow rearrangement of the network. This diffusive mechanism leads to more pronounced subdiffusion and more homogeneous transport than caging and hopping—exactly as we see for linear DNA in entangled versus crosslinked composites. Lastly, we previously showed that the more extreme subdiffusion seen in actin networks compared to microtubules was linked with more compact conformations due to more persistent trapping of particles. Likewise, we find that linear DNA assumes more compact conformations in entangled compared to crosslinked networks.

In summary, we have combined SMCT with ensemble DDM transport analysis to elucidate the transport properties of linear and ring DNA molecules within in vitro cytoskeleton networks. We reveal the intriguing role that DNA topology plays in transport and how this role varies with the introduction of crosslinking into cytoskeletal networks (Fig. 5). We find overwhelming evidence of

threading of ring DNA by cytoskeleton filaments, resulting in slow anomalous diffusion coupled with a heterogeneous ensemble of transport modes with corresponding swollen conformational states. Further, for ring DNA, crosslinking results in slower and more anomalous diffusion due to cytoskeleton filaments threading the rings and crosslinkers reducing the rate at which rings can be unthreaded via constraint release (*68*, *69*). In contrast, linear DNA displays faster and less subdiffusive transport that is largely homogeneous and coupled to more compact conformations compared to rings, indicating a single diffusive transport mode. Moreover, crosslinking the cytoskeleton network actually leads to faster and less subdiffusive dynamics along with more heterogeneous transport for linear DNA. This unexpected phenomenon likely arises from the increased rigidity of the network, which leads to caging and hopping rather than slow DNA transport coupled to the dynamics of the network.

Our collective results reveal the critical role that DNA topology plays in cytoskeleton transport and how altering cytoskeleton connectivity can enable a myriad of conformational and transport dynamics of biopolymers across scales. Specifically, we demonstrate the important role that threading could play in intracellular transport of ring DNA. Without crosslinkers, cytoskeleton filaments in cells can reptate to both thread and unthread molecules, resulting in threaded molecules that are largely immobile (i.e., confined by $R_G$ and $\xi$) and unthreaded ones that are more mobile. Even when crosslinkers are present, cytoskeleton filaments polymerize and depolymerize in cells, so there are situations where a crosslinked network could form in the presence of ring DNA and thread it, thereby immobilizing it. Beyond the biological implications of our work, our results provide key insights into the poorly understood physics of entangled and crowded ring polymers and topological polymer blends important to materials engineering and industrial applications.

## MATERIALS AND METHODS

### DNA

Double-stranded 115-kbp DNA was prepared through replication of bacterial artificial chromosomes in *Escherichia coli*, followed by purification and extraction as described previously (*46*). Following purification, supercoiled circular DNA was converted to linear and ring (relaxed circular) topologies through treatment with MluI and topoisomerase-I (New England Biolabs), respectively (*57*). In all experiments, DNA was fluorescent-labeled with YOYO-1 (Thermo Fisher Scientific) at a base pair to dye ratio of 4:1 (*58*).

### Cytoskeleton proteins

Composite networks of either entangled or crosslinked actin and microtubules were prepared using previously described protocols (*68*). Briefly, a 1:1 molar ratio of porcine brain tubulin dimers and rabbit skeletal actin monomers (Cytoskeleton) were resuspended to a final protein concentration of 5.8 μM in an aqueous buffer consisting of 100 mM PIPES, 2 mM $MgCl_2$, 2 mM EGTA, 1 mM adenosine 5′-triphosphate, 1 mM guanosine 5′-triphosphate, and 5 μM Taxol (*15*). Final solutions were pipetted into capillary tubing, sealed with epoxy, and incubated for 30 min at 37°C to polymerize proteins and form composite networks. For crosslinked composites, biotin-NeutrAvidin crosslinker complexes were preassembled as described previously (*68*) and added to the protein solutions at a crosslinker to protein molar ratio of $R_{CP} = 0.02$ before incubation (*68*). Both networks, fully characterized in (*15*) and (*68*), consist of randomly oriented filaments with minimal bundling and no phase separation between proteins (*15*, *68*). The composite mesh size is $\xi \approx 0.81$ μm (*15*). In the crosslinked composite, if we assume that all crosslinkers are incorporated in the network, then the length between crosslinkers along an actin filament would be $l_{c,a} = \frac{1}{2} l_{mon} \times R_{CP}^{-1} = 135$ nm, where $l_{mon} = 2.7$ nm is the length that each actin monomer adds to an actin filament. Similarly, the length between crosslinkers along a microtubule would be $l_{c,m} = \frac{1}{2}(l_{ring}/13) \times R_{CP}^{-1} = 30$ nm, where every 13 tubulin dimers add $l_{ring} = 7.8$ nm in length to the microtubule. These length scales are smaller than $\xi$, which would suggest bundling of filaments that would, in turn, increase the mesh size. However, we found no evidence of these effects in composites. We can therefore assume that there is a fraction of crosslinkers that remain free in solution and not incorporated into the network, which would increase $l_{c,a}$ and $l_{c,m}$ and thus limit bundling. While we cannot determine this fraction, given that $l_c$ is substantially smaller than $\xi$, we assume that every filament entanglement is permanently linked in the crosslinked composite.

### Sample preparation

For all experiments, YOYO-labeled linear or ring DNA was added to the protein solution before loading into capillary tubing at concentrations of 0.25 or 26 μg $ml^{-1}$ for single-molecule or DDM measurements, respectively. Glucose (0.9 mg $ml^{-1}$), glucose oxidase (0.86 mg $ml^{-1}$), and catalase (0.14 mg $ml^{-1}$) were also added to inhibit photobleaching. 0.05% Tween was added to prevent surface interactions.

### Imaging and analysis

DNA molecules within composites were imaged using a home-built light sheet microscope with a 10× 0.25 numerical aperture (NA) excitation objective, a 20× 0.5 NA imaging objective, and an Andor Zyla 4.2 CMOS (complementary metal-oxide semiconductor) camera.

#### *Single-molecule conformational tracking*

For each sample, 45 videos displaying ~10 DNA molecules per frame were recorded at 10 frames/s (fps) for 500 frames. All data presented are for an ensemble of ~1000 molecules from two different samples, each tracked for a minimum of 2.5 s. Custom-written software (Python) was used to track the COM positions ($x$, $y$) as well as the lengths of the major axis ($R_{max}$) and minor axis ($R_{min}$) of each molecule in each frame. From COM positions, we computed the MSD = $\frac{1}{2}(\langle(\Delta x)^2\rangle + \langle(\Delta y)^2\rangle)$ and corresponding transport coefficients and scaling exponents via MSD = $Kt^{\alpha}$ (Figs. 1B and 2 and fig. S1). From the major and minor axis length measurements, we calculated an effective coil size $R_{coil} = [\frac{1}{2}(R_{max}^2 + R_{min}^2)]^{\frac{1}{2}}$ (Figs. 1B and 3) (*19*). Lastly, we characterized the time-dependent conformational fluctuations of single molecules by calculating the fractional fluctuation length $L_f(t) = \langle|R_{max}(t) - R_{max}(0)|\rangle/\langle R_{max}\rangle$ for all lag times $t$. $L_f(t)$ quantifies the time scale and fractional length scale over which single molecules fluctuate between different conformational states. These analysis methods, depicted in Fig. 1, have been described and validated previously (*19*–*21*, *35*).

#### *Differential dynamic microscopy*

For each sample, eight videos with a 256 pixel × 1280 pixel (49.6 μm × 248.3 μm) field of view were recorded at 18 fps for 5000 frames at different regions within the sample. For DDM analysis [described in (*62*)], videos were then split into 256 pixel × 256 pixel (49.6 μm × 49.6 μm) ROIs (*19*, *62*–*64*). Each ROI was analyzed individually and averaged together after analysis (Fig. 1C). A two-dimensional (2D)

Fourier transform was taken from the difference between images separated by time lags of 0.05 to 166.55 s (Figs. 1C and 2). Because of dynamics are isotropic, the 2D Fourier transform was radially averaged for all lag times $t$, resulting in the DDM matrix $D(q,t)$, where $q$ is the magnitude of the wave vector. The DDM matrix can be fit to $D(q,t) = A(q)[1 - f(q,t)] + B(q)$, where $f(q,t)$ is the ISF. We used a stretched exponential for the ISF (fig. S2). While these fits for each $q$ do not follow the data over all $t$ for ring DNA, they did allow us to extract the parameters $A(q)$ and $B(q)$. With the measured $D(q,t)$ and extracted $A(q)$ and $B(q)$, we plotted the ISF, $f(q,t)$, for a particular wave vector to compare the rate at which the ISF decays (Figs. 1C and 3).

## SUPPLEMENTARY MATERIALS

Supplementary material for this article is available at http://advances.sciencemag.org/cgi/content/full/5/12/eaay5912/DC1

Table S1. Quantities derived from single-molecule conformational dynamics analysis.
Fig. S1. Distribution of individual MSDs from SMCT analysis.
Fig. S2. Fits to $D(q,t)$ from DDM analysis.

View/request a protocol for this paper from *Bio-protocol*.

## REFERENCES AND NOTES


1. R. J. Ellis, Macromolecular crowding: An important but neglected aspect of the intracellular environment. *Curr. Opin. Struct. Biol.* **11**, 114–119 (2001).
2. S.-i. Nakano, D. Miyoshi, N. Sugimoto, Effects of molecular crowding on the structures, interactions, and functions of nucleic acids. *Chem. Rev.* **114**, 2733–2758 (2014).
3. D. Miyoshi, N. Sugimoto, Molecular crowding effects on structure and stability of DNA. *Biochimie* **90**, 1040–1051 (2008).
4. C. Tan, S. Saurabh, M. P. Bruchez, R. Schwartz, P. LeDuc, Molecular crowding shapes gene expression in synthetic cellular nanosystems. *Nat. Nanotechnol.* **8**, 602–608 (2013).
5. S.-i. Nakano, N. Sugimoto, Model studies of the effects of intracellular crowding on nucleic acid interactions. *Mol. Biosyst.* **13**, 32–41 (2017).
6. M. L. Gardel, K. E. Kasza, C. P. Brangwynne, J. Liu, D. A. Weitz, in *Methods in Cell Biology*, vol. 89 of *Biophysical Tools for Biologists, Volume Two: In Vivo Techniques* (Academic Press, 2008), pp. 487–519; www.sciencedirect.com/science/article/pii/S0091679X08006195.
7. T. D. Pollard, The cytoskeleton, cellular motility and the reductionist agenda. *Nature* **422**, 741–745 (2003).
8. F. Huber, A. Boire, M. P. López, G. H. Koenderink, Cytoskeletal crosstalk: When three different personalities team up. *Curr. Opin. Cell Biol.* **32**, 39–47 (2015).
9. M. Kikumoto, M. Kurachi, V. Tosa, H. Tashiro, Flexural rigidity of individual microtubules measured by a buckling force with optical traps. *Biophys. J.* **90**, 1687–1696 (2006).
10. O. C. Rodriguez, A. W. Schaefer, C. A. Mandato, P. Forscher, W. M. Bement, C. M. Waterman-Storer, Conserved microtubule-actin interactions in cell movement and morphogenesis. *Nat. Cell Biol.* **5**, 599–609 (2003).
11. M. Dogterom, G. H. Koenderink, Actin–microtubule crosstalk in cell biology. *Nat. Rev. Mol. Cell Biol.* **20**, 38–54 (2019).
12. H. Kubitschke, J. Schnauss, K. D. Nnetu, E. Warmt, R. Stange, J. Kaes, Actin and microtubule networks contribute differently to cell response for small and large strains. *New J. Phys.* **19**, 093003 (2017).
13. E. E. Joo, K. M. Yamada, Post-polymerization crosstalk between the actin cytoskeleton and microtubule network. *BioArchitecture* **6**, 53–59 (2016).
14. Y. Yang, M. Bai, W. S. Klug, A. J. Levine, M. T. Valentine, Microrheology of highly crosslinked microtubule networks is dominated by force-induced crosslinker unbinding. *Soft Matter* **9**, 383–393 (2013).
15. S. N. Ricketts, J. L. Ross, R. M. Robertson-Anderson, Co-entangled actin-microtubule composites exhibit tunable stiffness and power-law stress relaxation. *Biophys. J.* **115**, 1055–1067 (2018).
16. S. N. Ricketts, M. L. Francis, L. Farhadi, M. J. Rust, M. Das, J. L. Ross, R. M. Robertson-Anderson, Varying crosslinking motifs drive the mesoscale mechanics of actin-microtubule composites. *Sci. Rep.* **9**, 12831 (2019).
17. Y.-C. Lin, G. H. Koenderink, F. C. MacKintosh, D. A. Weitz, Control of non-linear elasticity in F-actin networks with microtubules. *Soft Matter* **7**, 902–906 (2011).
18. V. Pelletier, N. Gal, P. Fournier, M. L. Kilfoil, Microrheology of microtubule solutions and actin-microtubule composite networks. *Phys. Rev. Lett.* **102**, 188303 (2009).
19. K. Regan, D. Wulstein, H. Rasmussen, R. McGorty, R. M. Robertson-Anderson, Bridging the spatiotemporal scales of macromolecular transport in crowded biomimetic systems. *Soft Matter* **15**, 1200–1209 (2019).
20. S. M. Gorczyca, C. D. Chapman, R. M. Robertson-Anderson, Universal scaling of crowding-induced DNA mobility is coupled with topology-dependent molecular compaction and elongation. *Soft Matter* **11**, 7762–7768 (2015).
21. C. D. Chapman, S. Gorczyca, R. M. Robertson-Anderson, Crowding induces complex ergodic diffusion and dynamic elongation of large DNA molecules. *Biophys. J.* **108**, 1220–1228 (2015).
22. E. Dauty, A. S. Verkman, Actin cytoskeleton as the principal determinant of size-dependent DNA mobility in cytoplasm. A new barrier for non-viral gene delivery. *J. Biol. Chem.* **280**, 7823–7828 (2005).
23. E. Dauty, A. S. Verkman, Molecular crowding reduces to a similar extent the diffusion of small solutes and macromolecules: Measurement by fluorescence correlation spectroscopy. *J. Mol. Recognit.* **17**, 441–447 (2004).
24. F. Höfling, T. Franosch, Anomalous transport in the crowded world of biological cells. *Rep. Prog. Phys.* **76**, 046602 (2013).
25. B. M. Regner, D. Vučinić, C. Domnisoru, T. M. Bartol, M. W. Hetzer, D. M. Tartakovsky, T. J. Sejnowski, Anomalous diffusion of single particles in cytoplasm. *Biophys. J.* **104**, 1652–1660 (2013).
26. E. E. Vaughan, J. V. DeGiulio, D. A. Dean, Intracellular trafficking of plasmids for gene therapy: Mechanisms of cytoplasmic movement and nuclear import. *Curr. Gene Ther.* **6**, 671–681 (2006).
27. J. J. Jones, J. R. C. van der Maarel, P. S. Doyle, Effect of nanochannel geometry on DNA structure in the presence of macromolecular crowding agent. *Nano Lett.* **11**, 5047–5053 (2011).
28. A. Zinchenko, DNA conformational behavior and compaction in biomimetic systems: Toward better understanding of DNA packaging in cell. *Adv. Colloid Interface Sci.* **232**, 70–79 (2016).
29. G. L. Lukacs, P. Haggie, O. Seksek, D. Lechardeur, N. Freedman, A. S. Verkman, Size-dependent DNA mobility in cytoplasm and nucleus. *J. Biol. Chem.* **275**, 1625–1629 (2000).
30. S. Zorrilla, M. A. Hink, A. J. W. G. Visser, M. P. Lillo, Translational and rotational motions of proteins in a protein crowded environment. *Biophys. Chem.* **125**, 298–305 (2007).
31. D. S. Banks, C. Fradin, Anomalous diffusion of proteins due to molecular crowding. *Biophys. J.* **89**, 2960–2971 (2005).
32. I. Y. Wong, M. L. Gardel, D. R. Reichman, E. R. Weeks, M. T. Valentine, A. R. Bausch, D. A. Weitz, Anomalous diffusion probes microstructure dynamics of entangled F-actin networks. *Phys. Rev. Lett.* **92**, 178101 (2004).
33. I. Lončarević, D. Dujak, Z. M. Jakšić, A. Karač, L. Budinski-Petković, S. B. Vrhovac, Anomalous tracer diffusion in the presence of extended obstacles on a triangular lattice. *Physica A* **527**, 121258 (2019).
34. R. M. Robertson, D. E. Smith, Self-diffusion of entangled linear and circular DNA molecules: Dependence on length and concentration. *Macromolecules* **40**, 3373–3377 (2007).
35. W. M. Mardoum, S. M. Gorczyca, K. E. Regan, T.-C. Wu, R. M. Robertson-Anderson, Crowding induces entropically-driven changes to DNA dynamics that depend on crowder structure and ionic conditions. *Front. Phys.* **6**, 53 (2018).
36. H. Kang, N. M. Toan, C. Hyeon, D. Thirumalai, Unexpected swelling of stiff DNA in a polydisperse crowded environment. *J. Am. Chem. Soc.* **137**, 10970–10978 (2015).
37. M. Doi, S. F. Edwards, *The Theory of Polymer Dynamics* (Clarendon Press, 1988).
38. P.-G. de Gennes, P. P.-G. Gennes, *Scaling Concepts in Polymer Physics* (Cornell Univ. Press, 1979).
39. M. Rubinstein, Dynamics of ring polymers in the presence of fixed obstacles. *Phys. Rev. Lett.* **57**, 3023–3026 (1986).
40. A. Grosberg, Y. Rabin, S. Havlin, A. Neer, Crumpled globule model of the three-dimensional structure of DNA. *Europhys. Lett.* **23**, 373–378 (1993).
41. S. P. Obukhov, M. Rubinstein, T. Duke, Dynamics of a ring polymer in a gel. *Phys. Rev. Lett.* **73**, 1263–1266 (1994).
42. M. Kapnistos, M. Lang, D. Vlassopoulos, W. Pyckhout-Hintzen, D. Richter, D. Cho, T. Chang, M. Rubinstein, Unexpected power-law stress relaxation of entangled ring polymers. *Nat. Mater.* **7**, 997–1002 (2008).
43. J. Suzuki, A. Takano, Y. Matsushita, Topological effect in ring polymers investigated with Monte Carlo simulation. *J. Chem. Phys.* **129**, 034903 (2008).
44. T. Vettorel, A. Y. Grosberg, K. Kremer, Statistics of polymer rings in the melt: A numerical simulation study. *Phys. Biol.* **6**, 025013 (2009).
45. T. Sakaue, Ring polymers in melts and solutions: Scaling and crossover. *Phys. Rev. Lett.* **106**, 167802 (2011).
46. R. M. Robertson, S. Laib, D. E. Smith, Diffusion of isolated DNA molecules: Dependence on length and topology. *Proc. Natl. Acad. Sci. U.S.A.* **103**, 7310–7314 (2006).
47. B. V. S. Iyer, A. K. Lele, S. Shanbhag, What is the size of a ring polymer in a ring–linear blend? *Macromolecules* **40**, 5995–6000 (2007).
48. J. D. Halverson, W. B. Lee, G. S. Grest, A. Y. Grosberg, K. Kremer, Molecular dynamics simulation study of nonconcatenated ring polymers in a melt. I. Statics. *J. Chem. Phys.* **134**, 204904 (2011).

49. Y. Zhou, K.-W. Hsiao, K. E. Regan, D. Kong, G. B. McKenna, R. M. Robertson-Anderson, C. M. Schroeder, Effect of molecular architecture on ring polymer dynamics in semidilute linear polymer solutions. *Nat. Commun.* **10**, 1753 (2019).
50. R. M. Robertson, D. E. Smith, Strong effects of molecular topology on diffusion of entangled DNA molecules. *Proc. Natl. Acad. Sci. U.S.A.* **104**, 4824–4827 (2007).
51. D. J. Orrah, J. A. Semlyen, S. B. Ross-Murphy, Studies of cyclic and linear poly(dimethylsiloxanes): 27. Bulk viscosities above the critical molar mass for entanglement. *Polymer* **29**, 1452–1454 (1988).
52. S. F. Tead, E. J. Kramer, G. Hadziioannou, M. Antonietti, H. Sillescu, P. Lutz, C. Strazielle, Polymer topology and diffusion: A comparison of diffusion in linear and cyclic macromolecules. *Macromolecules* **25**, 3942–3947 (1992).
53. G. B. McKenna, G. Hadziioannou, P. Lutz, G. Hild, C. Strazielle, C. Straupe, P. Rempp, A. J. Kovacs, Dilute solution characterization of cyclic polystyrene molecules and their zero-shear viscosity in the melt. *Macromolecules* **20**, 498–512 (1987).
54. Y.-B. Yang, Z.-Y. Sun, C.-L. Fu, L.-J. An, Z.-G. Wang, Monte Carlo simulation of a single ring among linear chains: Structural and dynamic heterogeneity. *J. Chem. Phys.* **133**, 064901 (2010).
55. D. G. Tsalikis, V. G. Mavrantzas, Threading of ring poly(ethylene oxide) molecules by linear chains in the melt. *ACS Macro Lett.* **3**, 763–766 (2014).
56. D. Michieletto, D. Marenduzzo, E. Orlandini, G. P. Alexander, M. S. Turner, Threading dynamics of ring polymers in a gel. *ACS Macro Lett.* **3**, 255–259 (2014).
57. C. D. Chapman, S. Shanbhag, D. E. Smith, R. M. Robertson-Anderson, Complex effects of molecular topology on diffusion in entangled biopolymer blends. *Soft Matter* **8**, 9177–9182 (2012).
58. K. Regan, S. Ricketts, R. M. Robertson-Anderson, DNA as a model for probing polymer entanglements: Circular polymers and non-classical dynamics. *Polymers* **8**, 336 (2016).
59. E. S. G. Shaqfeh, The dynamics of single-molecule DNA in flow. *J. Non Newton. Fluid Mech.* **130**, 1–28 (2005).
60. T. Cosgrove, M. J. Turner, P. C. Griffiths, J. Hollingshurst, M. J. Shenton, J. A. Semlyen, Self-diffusion and spin-spin relaxation in blends of linear and cyclic polydimethylsiloxane melts. *Polymer* **37**, 1535–1540 (1996).
61. F. L. McCrackin, J. Mazur, C. M. Guttman, Monte Carlo studies of self-interacting polymer chains with excluded volume. I. Squared radii of gyration and mean-square end-to-end distances and their moments. *Macromolecules* **6**, 859–871 (1973).
62. D. M. Wulstein, K. E. Regan, R. M. Robertson-Anderson, R. McGorty, Light-sheet microscopy with digital Fourier analysis measures transport properties over large field-of-view. *Opt. Express* **24**, 20881–20894 (2016).
63. R. Cerbino, V. Trappe, Differential dynamic microscopy: Probing wave vector dependent dynamics with a microscope. *Phys. Rev. Lett.* **100**, 188102 (2008).
64. F. Giavazzi, D. Brogioli, V. Trappe, T. Bellini, R. Cerbino, Scattering information obtained by optical microscopy: Differential dynamic microscopy and beyond. *Phys. Rev. E.* **80**, 031403 (2009).
65. D. M. Wulstein, R. McGorty, Point-spread function engineering enhances digital Fourier microscopy. *Opt. Lett.* **42**, 4603–4606 (2017).
66. M. Reufer, V. A. Martinez, P. Schurtenberger, W. C. K. Poon, Differential dynamic microscopy for anisotropic colloidal dynamics. *Langmuir* **28**, 4618–4624 (2012).
67. T. Sentjabrskaja, E. Zaccarelli, C. De Michele, F. Sciortino, P. Tartaglia, T. Voigtmann, S. U. Egelhaaf, M. Laurati, Anomalous dynamics of intruders in a crowded environment of mobile obstacles. *Nat. Commun.* **7**, 11133 (2016).
68. S. N. Ricketts, B. Gurmessa, R. M. Robertson-Anderson, *Advances in Cytoskeleton Research [Working Title]* (IntechOpen, 2019); www.intechopen.com/online-first/microscale-mechanics-of-plug-and-play-in-vitro-cytoskeleton-networks.
69. M. L. Gardel, J. H. Shin, F. C. MacKintosh, L. Mahadevan, P. Matsudaira, D. A. Weitz, Elastic behavior of cross-linked and bundled actin networks. *Science* **304**, 1301–1305 (2004).


**Acknowledgments:** We thank S. Ricketts for work in optimizing and characterizing actin-microtubule polymerization and crosslinking protocols. We thank G. Aguirre for help in analyzing data. **Funding:** This work was supported by NIH-NIGMS award no. R15GM123420 to R.M.R.-A. and R.J.M., AFOSR award no. FA9550-17-1-0249 to R.M.R.-A., ACS PRF award no. 57326-UNI10 to R.J.M., and NSF award no. CBET-1603925 to R.M.R.-A. **Author contributions:** R.M.R.-A. and R.J.M. conceived the project, guided experiments, analyzed and interpreted data, and wrote the manuscript. D.M.W. and K.E.R. performed experiments, analyzed data, and wrote the manuscript. J.G. analyzed data. **Competing interests:** The authors declare that they have no competing interests. **Data and materials availability:** All data needed to evaluate the conclusions in the paper are present in the paper and/or the Supplementary Materials. Additional data related to this paper may be requested from the authors.

Submitted 1 July 2019
Accepted 18 October 2019
Published 13 December 2019
10.1126/sciadv.aay5912

**Citation:** D. M. Wulstein, K. E. Regan, J. Garamella, R. J. McGorty, R. M. Robertson-Anderson, Topology-dependent anomalous dynamics of ring and linear DNA are sensitive to cytoskeleton crosslinking. *Sci. Adv.* **5**, eaay5912 (2019).

Science Advances

# Topology-dependent anomalous dynamics of ring and linear DNA are sensitive to cytoskeleton crosslinking

Devynn M. Wulstein, Kathryn E. Regan, Jonathan Garamella, Ryan J. McGorty and Rae M. Robertson-Anderson

*Sci Adv* **5** (12), eaay5912.
DOI: 10.1126/sciadv.aay5912